

## **EFFECT OF ADDITIONAL SHEAR STRAIN ON RECRYSTALLIZATION TEXTURE FORMATION IN A HOT ROLLED Al-Fe ALLOY**

\*K. Ihara<sup>1</sup>, T. Yamaguchi<sup>1</sup>, and K. Matsumoto<sup>2</sup>

<sup>1</sup>*Kobe Steel, LTD., Moka, Tochigi, Japan*  
(\*Corresponding author: [ihara.kentaro@kobelco.com](mailto:ihara.kentaro@kobelco.com))

<sup>2</sup>*Kobe Steel, LTD., Kobe, Hyogo, Japan*

### **ABSTRACT**

Al-Fe alloy sheets having layers with different strain components were produced by unlubricated hot rolling and the recrystallization texture formation during annealing was investigated in each layer. In this study, the strain component introduced by rolling was quantitatively evaluated by measuring degree of bending of an aluminum pin embedded in the sheet. The textures before and after annealing were investigated by the SEM-EBSD technique. It was clarified that, in the middle layer, where comparatively small shear strain was introduced,  $\beta$ -fiber subgrains and cube  $\{001\}\langle 100\rangle$  oriented subgrains were formed before annealing, and cube oriented recrystallized grains grew after annealing. On the other hand, in the surface layer, where large additional shear strain was introduced, shear texture components and cube oriented subgrains were formed before annealing, and shear texture was retained even after annealing, while cube oriented subgrains did not grow and were encroached. It was suggested that introduced strain components influenced the recrystallization texture formation by inducing different distribution of the subgrain size, stored strain energy and orientation relationship with surroundings before annealing.

### **KEYWORDS**

Hot-rolling, Shear strain, Recrystallization, Texture

## INTRODUCTION

The microstructure developed during the hot-rolling process of aluminum and aluminum alloys affect the mechanical properties of the final product sheets. Especially, the crystallographic orientation in the final product sheets affects the  $r$ -value and ears during deep drawing (Humphreys & Hatherly, 2004), then the texture control in the hot-rolling process is important. When the friction between the rolling roll and rolled sheet in the hot-rolling is large, both the rolling texture and recrystallization texture tend to be heterogeneous in the thickness direction. It is known in many rolled aluminum alloy sheets that the texture in the surface layer was different from that in the middle layer because of additional shear strain. It was reported that in the vicinity of the surface layer, where large additional shear strain was introduced, the shear texture  $\langle 111 \rangle$ /ND and  $\langle 110 \rangle$ //RD which contain components of  $\{111\} \langle 110 \rangle$  and  $\{001\} \langle 110 \rangle$  developed during rolling, and the shear texture developed even after recrystallization annealing (Sakai et al., 2002). Particularly, it is thought that the  $\langle 111 \rangle$ //ND texture contributes to improve the  $r$ -value and press formability (Inoue & Takasugi, 2007). Therefore, asymmetrical rolling and high friction rolling have been applied to improve formability of aluminum alloys by adding shear strain in the rolled sheets as deep as possible (Kamijo et al., 1972; Inoue et al., 2005). However, few researches have been focused on the microstructures and texture before annealing and thus, the detailed mechanism is still unclear how the texture after annealing is affected by the texture before annealing. In this study, the Al-Fe alloy of commercially pure aluminum was chosen as the first material to be studied in order to clarify the fundamental process of the recrystallization texture formation. The main purpose of this study is to clarify the effect of additional shear strain on the rolling and recrystallization textures in the hot-rolled sheets by analyzing the transition of microstructure and orientation distribution through recrystallization annealing.

## EXPERIMENTAL PROCEDURE

The chemical composition of the sample is shown in Table 1. The alloy is classified as the commercially pure aluminum. The ingot produced by the semicontinuous casting method was homogenized at 773 K for 14.4 ks at a heating rate of  $3.3 \times 10^{-2}$  K/s. A sample with a thickness of 40mm was cut out from the ingot, and was hot-rolled at 623K by 1- way 2- pass rolling. The rolling reduction was approximately 50% per pass. The exit temperature of the rolled sample was 599 K. Immediately after hot-rolling, the rolled sample was water quenched. Microstructures and texture after homogenization treatment and after hot-rolling were analyzed by an optical microscope (OM) , a scanning electron microscope (SEM), a transmission electron microscope (TEM) and SEM- electron back scattering diffraction (SEM-EBSD) technique. To estimate shear strain distribution introduced by hot- rolling, pure aluminum wire with a diameter of 3 mm was embedded in the center of the sample in width. Following the method of Sakai et al. (1988), the shear strain distribution was estimated by measuring the change in the cross-sectional shape of the embedded pin before and after rolling. The shear strain component  $\gamma$  was obtained by dividing the entire plate thickness into 20 equal parts. In addition, micro Vickers hardness test was carried at a load of 100 g in order to evaluate the distribution of stored strain in the thickness of the hot-rolled and water quenched sample. After hot-rolling and water quenching, the sample was annealed at 623 K for 7.2 ks in a salt bath and was water quenched. In order to analyze the formation of the recrystallization texture during annealing, short time annealing tests for 100s and 1000s were also carried at 623 K. Texture analyses were carried out with samples before and after annealing by a SEM-EBSD technique. The X-ray diffraction (XRD) technique was also used to measure the rolling texture. Measurement of texture by XRD was carried out on the surface of the rolled plane, quarter and middle layers which were obtained by polishing and etching. In the XRD technique, incomplete  $\{001\}$  and  $\{111\}$  pole figures were measured by the reflection method (measurement angle range:  $\alpha = 15$  to  $90^\circ$ ). The orientation distribution function, ODF, was calculated by the series expansion method. The expansion order of the even term was 22 and that of the odd term was 19. The orientation distribution analysis and ODF measurement was carried out by the SEM-EBSD method from the surface layer to the middle layer of the ND-RD cross section. The expansion order of ODF by SEM-EBSD was 22 and full width half maximum was 5 deg. Calculation of area fractions of each orientation component and orientation mapping was also conducted by SEM-EBSD technique, with the tolerance angle of 15 deg from the ideal orientation. Furthermore the analysis of the number fraction, the area fraction, and the average size of the each subgrain

orientation component in samples before and after annealing was conducted. In the analysis of a sample before annealing, approximately 1500–1700 subgrains in a 100  $\mu\text{m}$  square were employed and in the analysis of a sample after annealing, approximately 1000-1600 grains in a 1000  $\mu\text{m}$  square were employed.

Table 1. Chemical composition of Al-Mg-Si alloys studied (wt.%)

Si	Fe	Cu	Mn	Mg	Zn	Ti	Al
0.21	0.37	0.00	0.00	0.00	0.00	0.02	bal.

## RESULTS AND DISCUSSION

### Microstructure and Crystallographic Orientation Distribution after Homogenization Treatment

Figure 1 shows grain structure, Al-Fe-Si particles, dispersoids and ODF after the homogenization treatment. Grains were equiaxed in shape and the mean size was about 150  $\mu\text{m}$  in diameter. Al-Fe-Si particles were divided and spheroidized. Al-Fe-Si dispersoids were distributed sparsely. Orientation distribution was almost random.

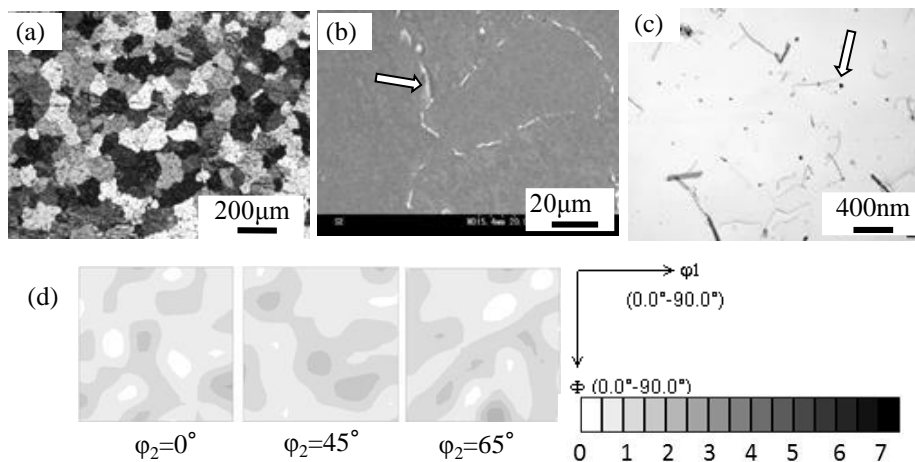


Figure 1. Microstructures after homogenization treatment, (a) Grain structure (OM), (b) Al-Fe-Si particles (SEM), (c) Al-Fe-Si dispersoids (TEM), (d) ODF by SEM-EBSD

### Distribution of Shear Strain, Hardness, and Grain Structure Introduced by Unlubricated Hot-Rolling

Figure 2 shows distribution of shear strain components, hardness, optical micrographs from the outermost surface to the middle layer, and SEM-EBSD maps in each layer after hot-rolling and water quenching. In Figure 2c, recrystallized grains were observed only near surface from the outermost surface to 100  $\mu\text{m}$  in depth. The area fraction of the recrystallized grain structure was 1–2% of the whole area in thickness. These recrystallized grains are presumed to be formed in a short period before water quenching after hot-rolling. The shear strain at the 1/4 layer was estimated to be a max value in the thickness and that at the middle layer the shear strain was almost 0. At the surface which contacted with the roll, the relationship between the velocity of the rolls and that of the sample reverse in front of and behind the neutral plane. Therefore, it is thought that the decrease of shear strain from 1/4 layer to surface in Figure 2a is apparent and the shear strain actually increases from the 1/4 layer to the middle layer. In Figure 2b, hardness was minimum at the middle layer and increased with distance from the middle layer. However, hardness at the outermost surface was lower than the inside because recrystallization already occurred at the outermost surface. It is suggested that the stored strain energy before annealing was minimum at the middle layer and increases with distance from the middle layer except the outermost surface. The distribution of the main orientation components and KAM map in the hot-rolled and water quenched sample are shown in Figure 2d. The area in Figure 2d looked like un-recrystallized structures in Figure 2c. It is thought that these observed grains were

subgrains with about 10  $\mu\text{m}$  in diameter because they were surrounded by not only high angle boundaries but also small angle boundaries. In the surface layer, many RW{001}<110> and Z{111}<110> orientation subgrains and a few Cube{001}<100> orientation subgrains coexisted. The distribution of the Cube orientation subgrains in the surface layer was similar to that in the 1/4 layer and the middle layer. Subgrains with shear texture components such as RW and Z in the 1/4 layer were quite fewer than that in the surface layer. In the middle layer, there was hardly any subgrains with the shear texture components. On the other hand, a number of the  $\beta$ -fiber orientation subgrains and Cube orientation subgrains were distributed in the 1/4 and middle layer.

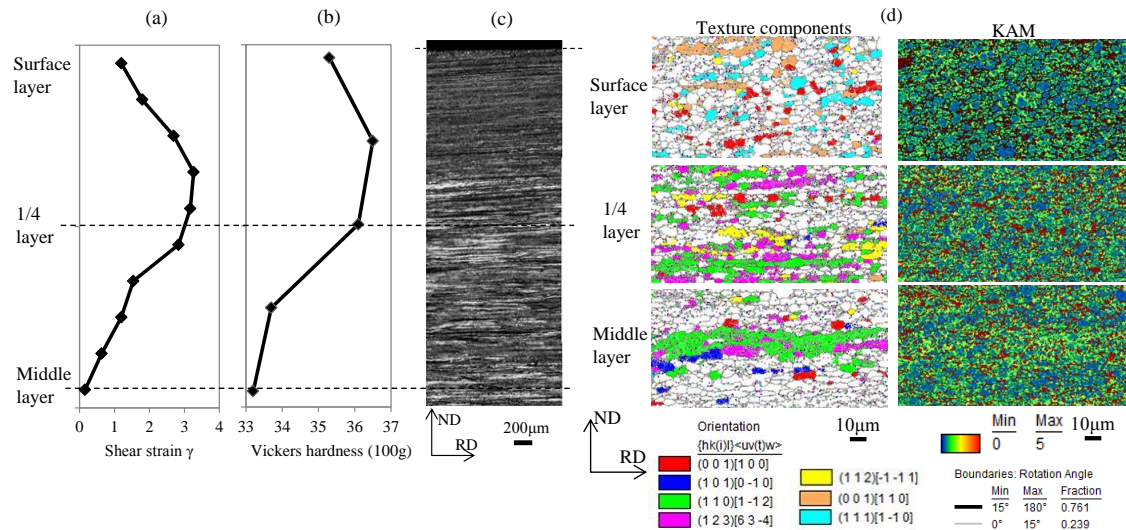


Figure 2. Shear strain, hardness and microstructures in hot-rolled sample before annealing, (a) shear strain, (b) micro-Vickers hardness, (c) optical microscope photograph, (d) SEM-EBSD maps

### Distribution of Al-Fe-Si Particles after Hot-Rolling

Figure 3 shows distribution of Al-Fe-Si particles at the surface, 1/4 and middle layer after unlubricated hot-rolling and water quenching. There were hardly any disparities in their size and number distribution.

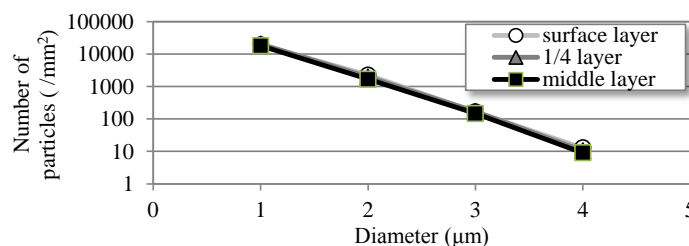


Figure 3. Distribution of Al-Fe-Si particles after hot-rolling and water-quench

### Texture after Hot-Rolling and Water Quenching

Figure 4 shows ODF by XRD in the surface, 1/4 and middle layer after unlubricated hot-rolling and water quenching. In the non-recrystallized surface layer, <110>//RD texture components such as the RW orientation and {111}//ND texture components such as the Z orientation were strongly accumulated. These textures were reported to be shear textures in aluminum alloys (Hölscher et al., 1994). In the 1/4 layer, the  $\alpha$ -fiber such as Brass{011}<211> and Goss{011}<100> orientation and the  $\beta$ -fiber such as S{123}<634>

and Cu{112}<111> orientation were accumulated, and the RW orientation, which is classified into shear texture were also slightly accumulated. In the middle layer, the shear texture was not accumulated. It is supposed this is because the shear strain was almost 0. Instead, the  $\alpha$ -fiber and  $\beta$ -fiber orientations were strongly accumulated.

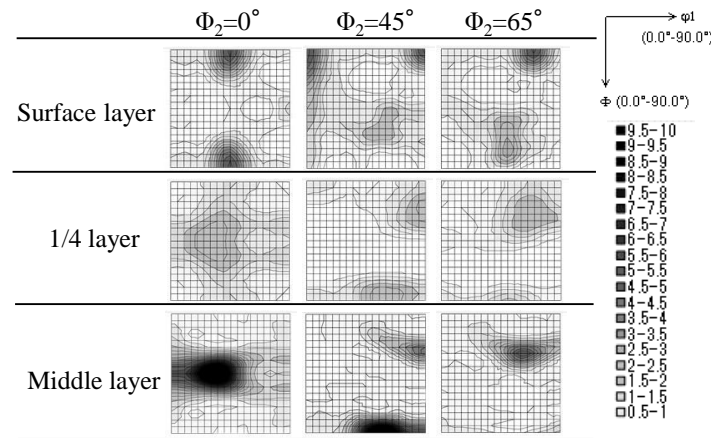


Figure 4. ODF after hot-rolling and water quenching (XRD)

### Microstructure and Texture after Recrystallization Annealing

Figure 5 shows the SEM-EBSD maps after annealing at 623 K for 7.2 ks and water quenching. Figure 5a shows normal direction (ND) orientation map and Figure 5b shows the distribution of main orientation components in the same area as Figure 5a. After annealing, in the surface layer, recrystallized grains with the shear texture such as RW and Z orientations were formed. On the other hand, in the 1/4 and middle layer, recrystallized grains with near the  $\beta$ -fiber texture components and near-Cube orientation were formed. Recrystallized grains with the  $\beta$ -fiber texture components contain the R orientation near-S orientation. The size of recrystallized grains became finer with distance from the middle layer. It is considered that the factor which affects the recrystallized grain size is the stored strain energy, the distribution of large particles (>1  $\mu\text{m}$ ) and fine dispersoids; the stored strain energy before annealing could be a driving force for recrystallization and grain growth, large particles could be nucleation sites of recrystallization which occurs by the particle stimulated nucleation (PSN), fine dispersoids could have the pinning effect to moving recrystallization boundaries. In this study, there were hardly any disparities in their size and number distribution of large particles shown in Figure 3 and fine Al-Fe-Si dispersoids had almost no effect to retard recrystallization because of the size and spacing shown in Figure 1c. On the other hand, it is deduced from the distribution of hardness shown in Figure 2b that the stored strain energy before annealing increased with distance from the middle layer. Therefore, it is presumed that the through-thickness variation of the recrystallized grain size shown in Figure 5 was due to the stored strain energy.

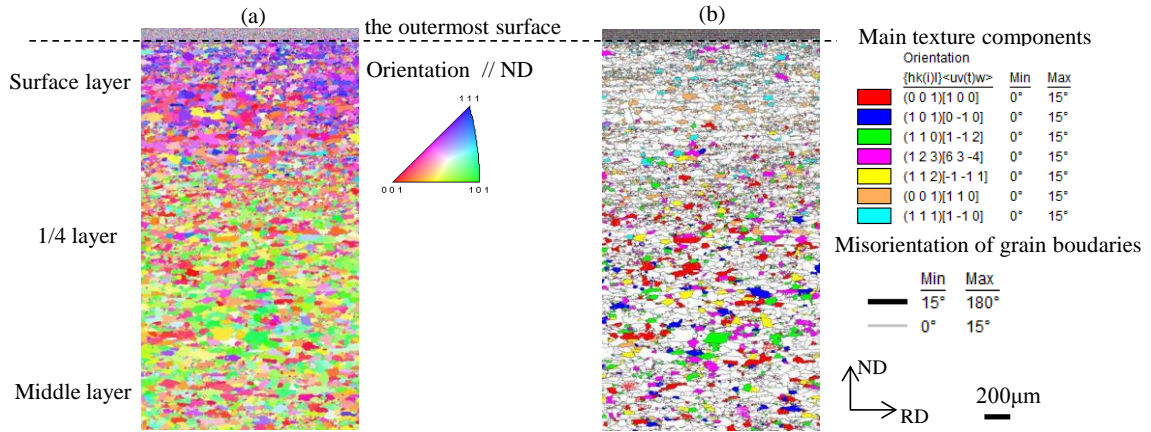


Figure 5. SEM-EBSD maps after annealing (623 K, 7.2 ks) (a) The distribution of orientation parallel to ND, (b) Main texture components distribution

### Recrystallization Texture Development Process

Figure 6 shows the ND orientation map in samples before and after annealing at 623 K for 100 s to 7.2 ks. The color in the map corresponds to that in the standard stereo triangle. In the surface layer, the orientation distribution of recrystallized grains was similar to that of un-recrystallized grains before annealing. In the 1/4 and middle layer, the minor orientation components represented by the near-red color before annealing increased after annealing. These changes of orientation distribution were shown more clearly in ODF shown in Figure 7. In the surface, the shear texture components such as RW and Z orientations distributed before annealing remained, while the Cube orientation disappeared after annealing for 7.2 ks. In the middle layer, although the  $\beta$ -fiber texture distributed before annealing became less accumulated, the Cube texture developed after annealing for 7.2 ks. Despite of difference in the introduced shear strain, the Cube texture developed similarly in the 1/4 and middle layer.

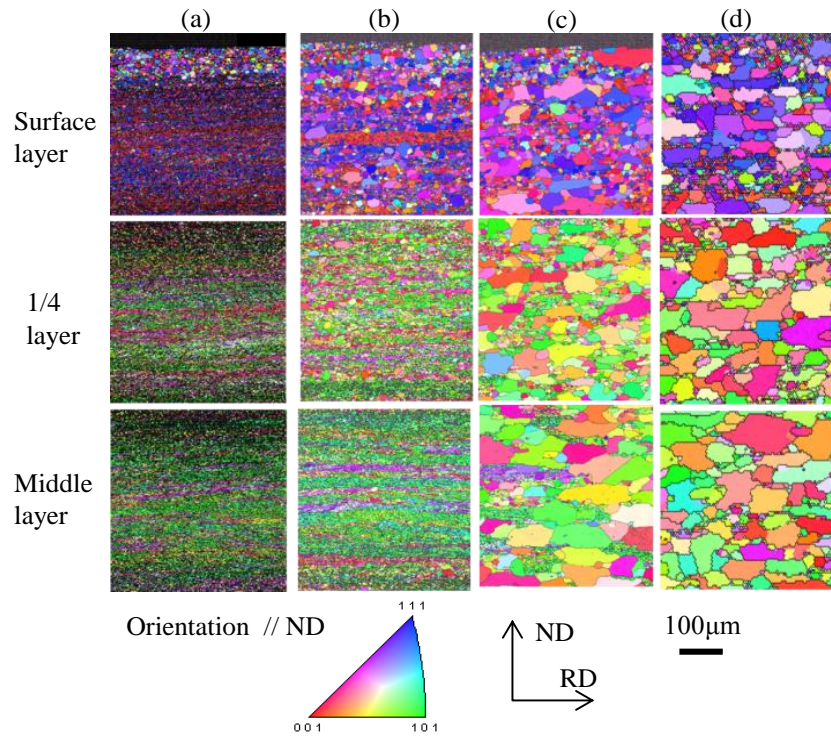


Figure 6. EBSD maps before and after 623K annealing (a) Before annealing, (b) 100 s, (c) 1000 s, (d) 7.2 ks

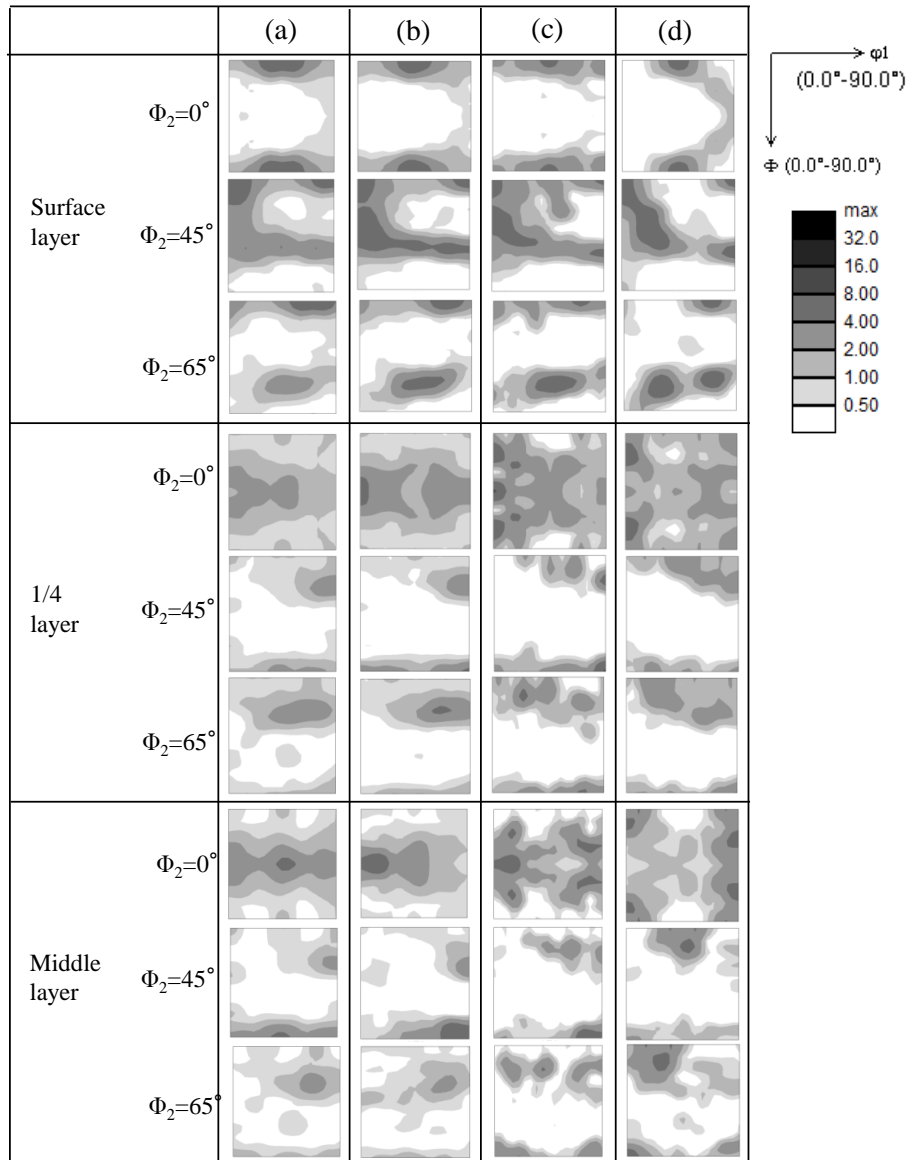


Figure 7. ODF before and after 623K annealing (a) Before annealing, (b) after 100 s, (c) after 1000 s, (d) after 7.2 ks

### Distribution of Main Texture Components before and after Annealing

Figures 8a and 8b show the number fraction and the area fraction of the main texture components and Figures 9a and 9b show the mean subgrain/grain size of the main texture components before and after annealing at 623 K for 7.2 ks. In the surface, the number and area fraction of the shear texture components such as RW and Z were larger than those of other components before and after annealing. There was no prominent difference in recrystallized grain size between texture components after annealing, although the subgrains for these shear texture components were slightly larger than those for other components before annealing. It is supposed that the above-mentioned feature in the surface layer was made because of the larger stored strain energy and the more rapid recrystallization than the other layer before annealing. Therefore, there is a possibility that it was easy for subgrains containing shear texture components in the surface layer to grow almost concurrently and to become finer recrystallized grains than other layers. It was reported by Inoue

et al. (2012) that the lower stored strain energy and  $40^\circ\langle 111 \rangle$  orientation relationship with the surrounding  $\{013\}\langle 631 \rangle$  subgrains contributed to growth of the typical shear texture component  $\{111\}\langle 110 \rangle$  grains in warm asymmetry rolled 6022 aluminum alloy sheet. In this study,  $\{111\}\langle 110 \rangle$  subgrains seems to have lower stored strain energy than surrounding subgrains in unlubricated hot-rolled Al-Fe alloy sample because there were a lot of  $\{111\}\langle 110 \rangle$  subgrains with lower KAM value than surrounding subgrains as shown in Figure 2d. However, the contribution of orientation relationship  $40^\circ\langle 111 \rangle$  between  $\{111\}\langle 110 \rangle$  and  $\{013\}\langle 631 \rangle$  in this study was obscure because the accumulation of  $\{013\}\langle 631 \rangle$  was very weak. On the other hand, in the 1/4 and middle layer, in which  $\beta$ -fiber orientation subgrains had large number and area fraction before annealing, it is supposed that the stored strain energy was lower than that in the surface layer. After annealing, especially the area fraction of Cube orientation grains increased and the number and area fraction of the  $\beta$ -fiber orientation grains decreased in the 1/4 and middle layer. In these layers, it is suggested that the condition for preferential growth of the Cube orientation subgrains which were the minor orientation components with a few number and area fraction was formed before annealing. The preferential growth of the Cube orientation subgrains was discussed in the next chapter.

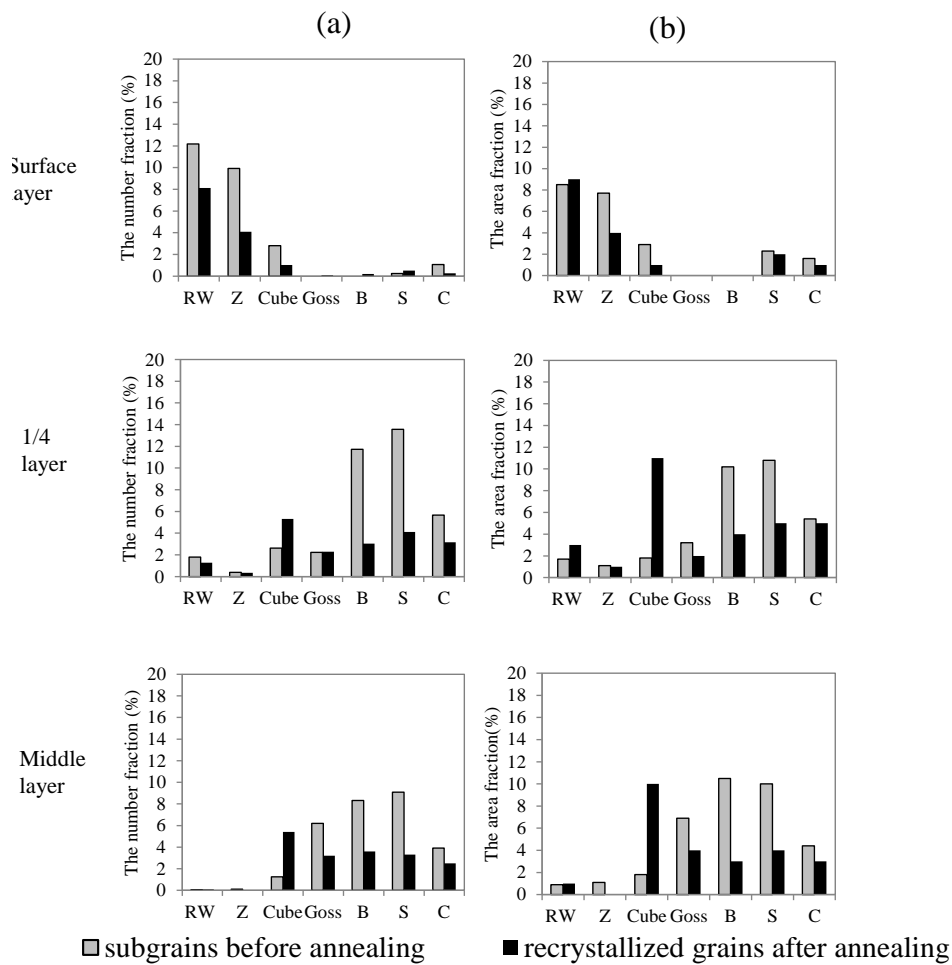


Figure 8. Number fraction and the area fraction of the main texture components before and after annealing at 623 K for 7.2 ks (a) Number fraction, (b) Area fraction

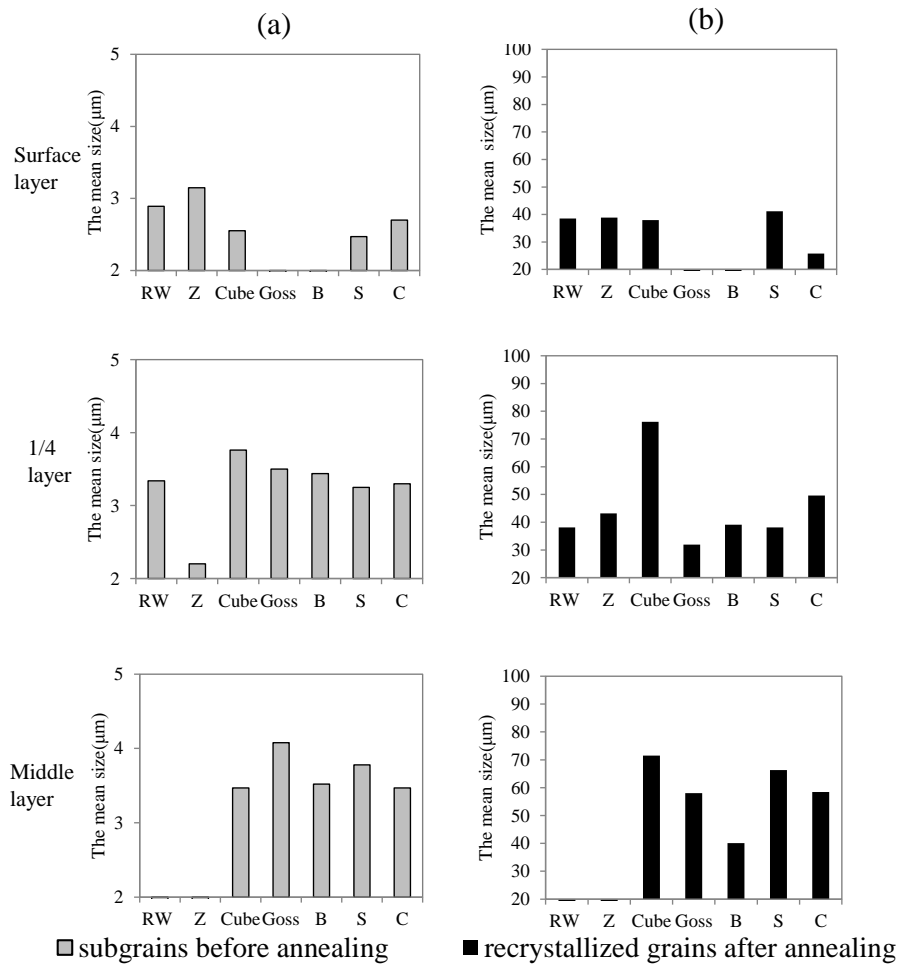


Figure 9. The mean subgrain/grain size of the main texture components before and after annealing at 623 K for 7.2 ks (a) mean subgrain size (diameter), (b) mean recrystallized grain size (diameter)

### Growth of Cube Oriented Subgrains in the 1/4 and Middle Layer of Hot-Rolled Al-Fe-Alloy Sample

In the unlubricated hot-rolled and water quenched sample, the Cube orientation subgrains were formed not only in the middle layer, where additional shear strain was almost 0, but also in the surface and 1/4 layer, where the shear strain was introduced. It was reported by Lee et al. (1994) that there is a possibility that the Cube orientation subgrains is formed when the shear strain is introduced moderately. It is possible that the Cube orientation microstructures in the examined alloy were formed by hot-rolling. However, the reason why the number and area fraction of the Cube orientation subgrains were similar in each layer in spite of the through-thickness variation of shear strain is still not solved. Figures 10a and 10b show the number fraction of the Cube orientation subgrains with the lowest KAM value and with the largest size in the neighbor area before annealing. The stored strain energy in subgrains with the lowest KAM value is considered to be lowest in the neighbor area. The number fraction of the Cube orientation subgrains with lowest KAM value in the 1/4 and middle layer were larger than that in the surface layer. In addition, the number fraction of the Cube orientation subgrains with the largest size in the neighbor area increased toward the middle layer. Furthermore, a number of the  $\beta$ -fiber orientation subgrains were distributed around the Cube orientation subgrains in the 1/4 and middle layer because shear strain in these layers was smaller than that in the surface layer. It was reported that the microstructure with the  $\beta$ -fiber orientation such as S orientation was easy to be encroached by the Cube orientated grains (Humphreys & Hatherly, 2004). As mentioned above, in the 1/4 and middle layer, it is

suggested that the condition for preferential growth of the Cube orientation subgrains not only in the size and stored strain energy but also orientation relationship with surrounding subgrains was formed.

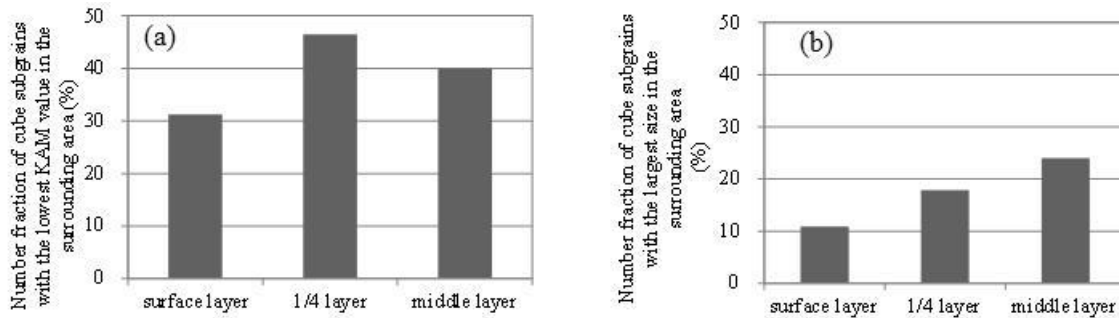


Figure 10. Number fraction of cube subgrains in the surrounding area before annealing (a) with the lowest KAM value, (b) with the largest size

## CONCLUSIONS

The development of the orientation distribution during recrystallization annealing was studied to clarify the effect of additional shear strain on the recrystallization texture formation in a hot-rolled Al-Fe alloy. The following conclusions were drawn:

- (1) In the surface layer, where large shear strain was introduced, the strong shear texture was developed before and after annealing. The Cube orientation subgrains, which were distributed slightly before annealing could not grow to recrystallized grains.
- (2) It was suggested that large shear strain and large stored strain energy contribute to develop the recrystallization texture in the surface layer.
- (3) In the layer with a small quantity of additional shear strain, the  $\beta$ -fiber texture which was developed before annealing became weakened after annealing. On the other hand, the Cube orientation subgrains which were distributed slightly grew preferentially.
- (4) In the layer with a small quantity of additional shear strain, it is suggested that the condition for the preferential growth of the Cube orientation subgrains was related not only to the size and the stored strain energy but also orientation relation with surrounding subgrains.

## REFERENCES

- Hölscher, M., Raabe, D. and Lücke, K. (1994). Relationship between rolling textures and shear textures in f.c.c. and b.c.c. metals. *Acta Metallurgica et Materialia*, 42, 879-886.
- Humphreys, F. J. & Hatherly, M. (2004). *Recrystallization and Related Annealing Phenomena* (2nd Ed.). Elsevier, Oxford.
- Inoue, H. (2012). Texture control of aluminum and magnesium alloys by the symmetric/asymmetric combination rolling process. *Materials Science Forum*, 702-703, 68-75.
- Inoue, H and Takasugi, T. (2007). Texture control for improving deep drawability in rolled and annealed aluminum alloy sheets. *Materials Transactions*, 48, 2014-2022.
- Inoue, H., Yamasaki, T., Gottstein, G., Van Houtte, P. and Takasugi, T. (2005). Recrystallization texture and r-value of rolled and T4-treated Al-Mg-Si alloy sheets. *Materials Science Forum*, 495-497, 573-578.
- Kamijo, T., Sekine, K., Matsukawa, Y., Noguchi, N. (1972). Rolling and annealing texture in the outer layer of rolled aluminum sheets. *Journal of the Japan Institute of Metals and Materials*, 36, 669-673.

- Lee, C.S., Smallman, R.E. & Duggan, B. J. (1994). Effect of rolling geometry and surface friction on cube texture formation. *Materials Science and Technology*, 10, 149-154.
- Sakai, T., Saito, Y., Hirano, K. & Kato, K. (1988). Deformation and recrystallization behavior of low carbon steel in high speed hot rolling. *Transactions ISIJ*, 28, 1028-1035.
- Sakai, T., Utsunomiya, H. & Saito, Y. (2002). Introduction of shear strain to aluminum alloy sheet and control of texture. *Journal of Japan Institute of Light Metals*, 52, 518-523.